



Kent Academic Repository

Martínez Jiménez, Alejandro, Grelet, Sacha, Tsaturian, Veronika, Montague, Patrick Bowen, Bradu, Adrian and Podoleanu, Adrian (2022) 400 Hz volume rate swept-source optical coherence tomography at 1060 nm using a KTN deflector. IEEE Photonics Technology Letters . p. 1. ISSN 1041-1135.

Downloaded from

<https://kar.kent.ac.uk/97311/> The University of Kent's Academic Repository KAR

The version of record is available from

<https://doi.org/10.1109/LPT.2022.3212015>

This document version

Author's Accepted Manuscript

DOI for this version

Licence for this version

CC BY (Attribution)

Additional information

Versions of research works

Versions of Record

If this version is the version of record, it is the same as the published version available on the publisher's web site. Cite as the published version.

Author Accepted Manuscripts

If this document is identified as the Author Accepted Manuscript it is the version after peer review but before type setting, copy editing or publisher branding. Cite as Surname, Initial. (Year) 'Title of article'. To be published in **Title of Journal**, Volume and issue numbers [peer-reviewed accepted version]. Available at: DOI or URL (Accessed: date).

Enquiries

If you have questions about this document contact ResearchSupport@kent.ac.uk. Please include the URL of the record in KAR. If you believe that your, or a third party's rights have been compromised through this document please see our [Take Down policy](https://www.kent.ac.uk/guides/kar-the-kent-academic-repository#policies) (available from <https://www.kent.ac.uk/guides/kar-the-kent-academic-repository#policies>).

400 Hz volume rate swept-source optical coherence tomography at 1060 nm using a KTN deflector

Alejandro Martínez Jiménez, Sacha Grelet, Veronika Tsaturian, Patrick Bowen Montague, Adrian Bradu, Adrian Podoleanu

Abstract—In this Letter, a swept-source optical coherence tomography (SS-OCT) instrument employing an innovative scanning protocol for high-speed volumetric rate imaging is demonstrated. The optical source is a tunable laser based on a supercontinuum source pumped with femtosecond pulses, followed by a time-stretched delay fiber. The instrument is equipped with an ultra-fast lateral scanner, based on a KTN crystal, driven at 100 kHz. The paper proves the utility of combining an ultra-fast lateral scanner with an ultra-fast swept laser to provide A-scans at a repetition rate of 40 MHz and an unprecedented 3D-OCT volume acquisition rate of 400 Hz.

Index Terms—OCT, electro-optic modulator, fast imaging, swept source

I. INTRODUCTION

IN optical coherence tomography (OCT), the speed of operation is determined by how fast data for axial reflectivity profiles (A-scans/s) are produced. The swept-source (SS) principle allowed an increase in the A-scan rate from a few Hz to hundreds of MHz [1]. For N_x pixels along the fast direction of lateral scanning with a sweeping rate of f , the line rate of the fast (line) scanner is f/N_x . Therefore, with a sweeping rate f of tens of MHz, and a need to have a few hundred N_x points laterally in the image, the lateral scanning rate must exceed tens of kHz. So far, in scanning OCT systems galvanometer-scanners are typically used. For faster speeds, resonant scanners can be harnessed, but they are only available up to a few tens of kHz. In a previous report using a frequency domain mode locked laser (FDML), a resonant scanner was employed [2], enabling volume rates up to 192.5 Hz. Alternatively, full-field OCT configurations could be used to increase volume rate without need of scanners, shifting the speed limitation to the camera sensor, leading to 116 Hz volume rate [3]. Increasing the tuning speed also requires further progress in the deflector technology for lateral scanning. If a multi-MHz swept-source is paired with a galvo or resonant scanner, data will be oversampled along the fast-scanning direction. For larger sweeping frequencies, lateral scanning faster than that provided by resonant scanners is needed. A $KTa_{1-x}Nb_xO_3$ (KTN), crystal-based optical deflector is capable of an order of magnitude faster scanning than resonant scanners. KTN as sample beam deflector has already been reported in a TD-OCT

The authors acknowledge the support of the Marie Curie Training ITN NETLAS-860807.

A. Martínez Jiménez, S. Grelet, V. Tsaturian, A. Bradu and A. Podoleanu are with School of Physical Sciences, University of Kent, United Kingdom.

S. Grelet and P. Bowen Montague are with NKT Photonics, Birkerød, Denmark.

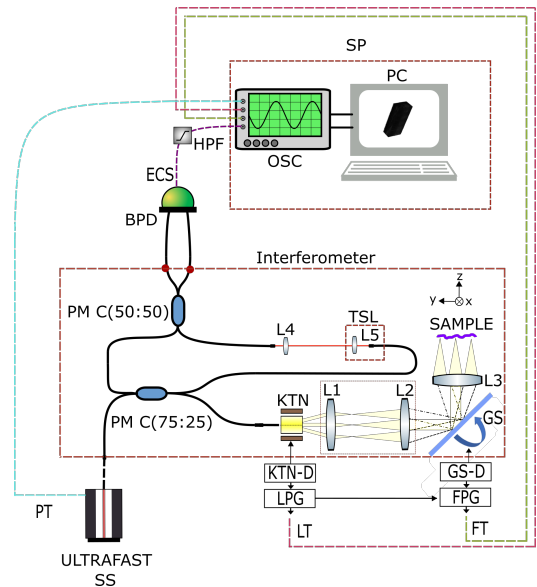


Fig. 1. **Experimental set-up.** SS: swept source; Interferometer (KTN: beam deflector, GS: galvanometer scanner, PM C: polarization maintaining couplers, TSL: translation stage launcher); SP: signal processing block (BPD: balanced photodetector, PDS: Photodetected signal, HPF: High pass filter, OSC: oscilloscope, PC: Personal computer); Triggers (LT: line, FT: frame, PT: Optical pulse); Pulse generators (LPG: line, FPG: frame); Drivers (KTN-D: KTN, GS-D: galvanometer scanner). Lenses: L1, L2, L3, L4 and L5 of focal lengths 3 cm, 7.5 cm, 4.5 cm, 1.5 cm and 1.5 cm respectively.

systems [4]. Its fast operation was also employed in a spectral filter to tune the output wavelength in a swept source [5]. In this paper, the tuning rate of the SS employed is $f = 40$ MHz. Therefore, an ultrafast deflector based on a KTN crystal driven by a 100 kHz sinusoidal waveform was utilized. As a result, during each half period of the sinusoidal driving signal applied to the KTN crystal, each fast line (T-scan) contains $N_x = 200$ points. To the best of our knowledge, this is the first report of a KTN scanner being used for sample beam scanning in a SS-OCT system. The swept-source utilized is based on the time-stretch principle, which uses a controlled amount of chromatic dispersion to enlarge a short broadband pulse, to a desired duration. Due to the different speeds at which different wavelengths travel through a dispersive element, sweeping in time is achieved without any active tuning. Thus, the repetition of sweeping events f , is defined by the repetition rate of pulses launched into the dispersive element.

Since the first report on time-stretch based SS-OCT by Moon et al. [6] at 5 MHz, other research groups reported increased sweeping rates using different techniques achieving

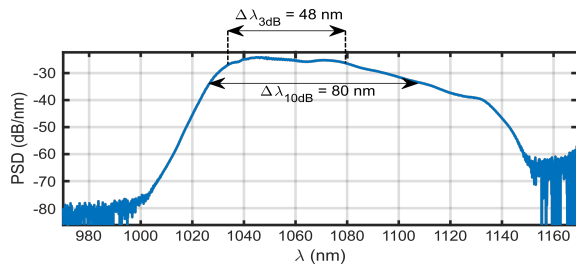


Fig. 2. **Output spectrum** of the supercontinuum time-stretched swept source used in this work.

up to 400 MHz [1]. Most recent reports in time-stretch swept sources have been produced in the telecommunication bandwidth due to the low losses of dispersing compensated fiber used for time-stretching. Here we present a system operating at a more amenable wavelength for biomedical imaging applications, of 1060 nm [7].

II. METHODS

A schematic diagram of the SS-OCT instrument is shown in Fig. 1, consisting of an ultrafast swept-source, interferometer and signal processing block. The SS employed here is operating at 40 MHz providing an average optical power of 20 mW. The spectrum is centered at 1060 nm and has 48 nm and 80 nm bandwidths at 3 dB and 10 dB respectively, as shown in Fig. 2. The SS design, based on supercontinuum generation followed by a time-stretch stage, is described in detail in [8], with the difference of a 40 MHz seed laser. The supercontinuum is generated in a polarization maintaining (PM) all-normal dispersion fiber (NL-1050-NEG-1-PM by NKT Photonics) and the pulses are stretched using 2.8 km of single mode fiber (980-XP by Nufern). The supercontinuum spectrum is generated by a coherent broadening mechanism [9]. As a consequence, the relative intensity noise of less than 1% is determined by the noise of the pump laser. Pulses of 1 ps duration are stretched up to 12 ns.

The interferometer employs two PM fiber-based couplers (PANDA PM980 XP by Nufern) of 25/75 and 50/50 coupling ratios and, 25% of the optical power is guided towards the sample via two lateral scanning devices: a KTN deflector (KTN by NTT Advanced Technology Corporation) for fast line scanning; and a galvanometer scanner (6210H by Cambridge Technology) for frame scanning. The deflection angle of the KTN scanner is proportional to the voltage applied, and is controlled by a high voltage signal delivered by a KTN driver (KPS1001CH-00 by NTT Advanced Technology Corporation). The maximum deflected angle is given by the 220 V applied to the crystal, which is fundamentally limited by the thickness of the crystal block [10]. Due to the dependence of deflection angle on the polarization state, the KTN crystal is coupled to a suitably oriented PM fiber. Effectively, if the back-scattered light experiences a polarization change, the collected signal may be reduced. Moreover, PM fibers only maintain one linear polarization, therefore interference will only occur if the back-scattered light is aligned with it. The beam shape distortion inside the KTN crystal is compensated by a cylindrical concave lens that reduces the astigmatism and produces a round

beam of 1 mm diameter. In order to improve the transversal resolution, the beam is enlarged using a telescope made of two achromatic lenses of 30 mm and 75 mm focal length in the telescope. Finally a 45 mm focal length lens is used to focus the fan of rays onto the sample.

The output optical signal was collected with a 23 GHz bandwidth balanced photodetector (BPR-23-M by Optilab) producing a photodetected signal (PDS), digitized by a 20 GHz bandwidth oscilloscope (Wavemaster 820Zi-b by Lecroy Teledyne). Pulsations given by the pulse repetition rate of the swept source at 40 MHz were eliminated by a 300 MHz high pass filter. The oscilloscope data was collected at 40 GS/s and transferred to a PC for processing.

A common issue in SS-OCT is that, due to nonlinear tuning and dispersion in the interferometer, the PDS signal is usually chirped. Therefore, different methods, such as phase calibration dispersion compensation (PCDC) and Complex Master Slave (CMS) signal processing [11] have been reported. For its ability to deliver *en-face* views without the need to slice the volume of data, the CMS method was chosen here. For calibration purposes, whilst using a flat mirror as a sample, several experimental PDS signals (of time duration equal to that of a single sweep of the laser across its spectral range) were collected for several optical path difference (OPD) values between the arms of the interferometer. In the setup in Fig. 1, 30 PDS signals were acquired for 30 OPD values equidistantly separated by 5 μm . The OPD was adjusted by actuating on the translation stage launcher. In Fig. 3(a) an example of a PDS corresponding to a single sweep is presented. Using these experimentally collected spectra, the calibration functions g and h , describing the nonlinearity in the tuning and the unbalanced dispersion between the arms of the interferometer, are presented respectively. The values for g and h were calculated using the procedure described in [12]. Subsequently, the two functions g and h , shown in Fig. 3(b), were employed to theoretically infer interferometric signals (masks). By multiplying the masks with the PDS for each sweep, (corresponding to each lateral pixel acquired while performed the lateral scanning over samples) cross-sectional and *en-face* images are produced. To implement the protocol used in [12], a MATLAB based software has been developed.

III. RESULTS

Figure 3 illustrates the depth resolution capabilities of the proposed instrument. The axial resolution is evaluated as $\delta z = 10 \mu\text{m}$ calculated for a 48 nm gaussian shape. Furthermore, the A-scan peaks in the Fig. 3(d) display constant width across the entire axial range with a sensitivity profile decay rate of 8 dB/mm. An attenuation of 6 dB is obtained for an axial range Δz of 0.61 mm in depth along coordinate Z . Near OPD = 0, a signal to noise ratio of ~ 45 dB is achieved. Figure 3(b) also shows that the chirp in the channeled spectrum modulation is mainly created by the dispersion, as the g function is almost linear. Since the sensitivity is currently insufficient to produce images from biological scattering samples, instead the imaging capability is demonstrated using the topography of a coin.

To perform imaging, the KTN driver delivered 200 V amplitude sinusoidal driving voltage at 100 kHz, producing

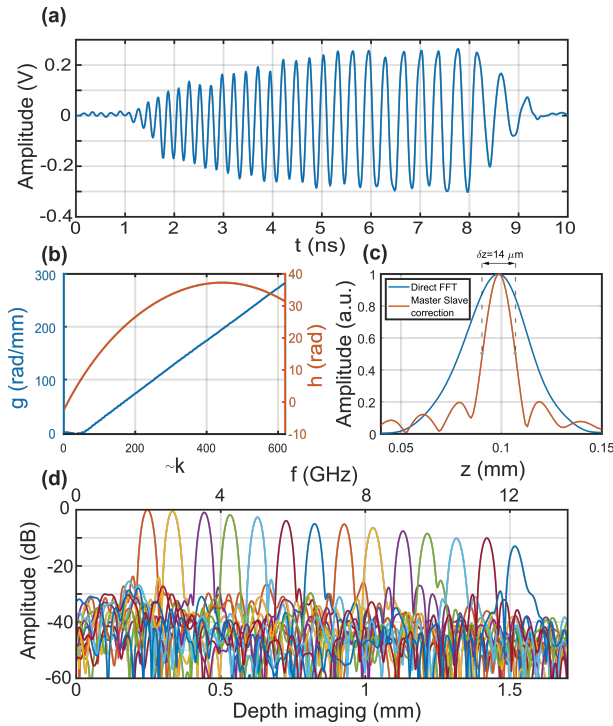


Fig. 3. **Calibration:** (a) Photodetected signal corresponding to a sweep. (b) g and h calibration functions obtained by CMS. (c) Comparison between FFT of uncorrected photodetected signal (blue) and corrected by CMS (red). (d) A-Scans obtained by CMS at 14 different OPD values.

a full detection angle of 124 mrad that covered 2.95 mm along X-direction. The image formed by the two scanners comprises a raster of N_y lines, with each line consisting of N_x points. Considering the period of 10 μs of the sinusoidal signal applied to the KTN crystal, this determines $N_y = 250$ horizontal lines in the frame. The lateral resolution, measured using an USAF target, is 23 μm in the x -direction and 18 μm along the y -direction. The different resolution along the x and y axes is expected due to imperfect compensation of the beam astigmatism introduced by the KTN crystal, only partially reduced by the cylindrical lens installed by the manufacturer at the output of the KTN crystal. These lateral resolutions are similar to those reported by previous works using a KTN for sample beam scanning [4]. The galvanometer-scanner is driven by a 400 Hz sawtooth signal with an amplitude of 2.5 Vpp, that determines an image size of 6.6 mm in the Y-direction. In the images presented Fig.4-6 only half ramp of the KTN is used. A higher framerate could be used to increase the volume rate, moreover both ramps of the KTN could be used if lateral resolution is adjusted. However, galvanometer scanners operation at higher frequencies could limit the lateral size. The oscilloscope data acquisition was triggered with the pump laser pulses. The trigger signals from the KTN, and galvanometer-scanner driver signal, were acquired synchronously with the photodetected signal during one period of the frame trigger signals (2.5 ms). Given a minimum dynamic range of 12 bits, more than 13 GB of data were generated in 2.5 ms. Since such a large amount of data cannot be transferred in real time, it was stored on the oscilloscope hard drive and subsequently

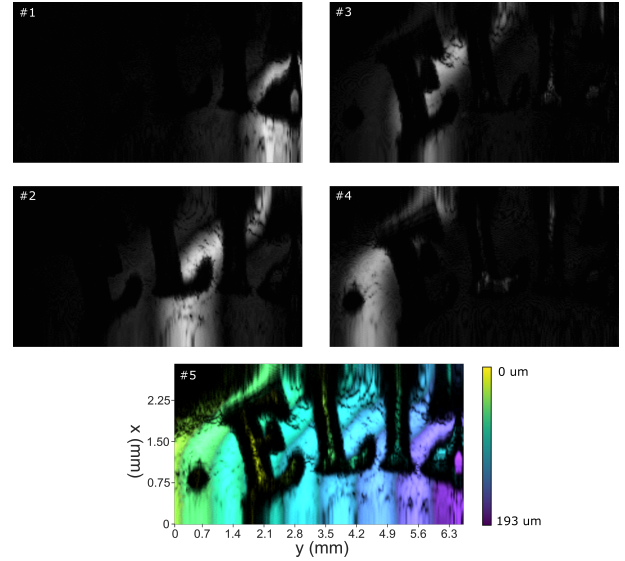


Fig. 4. **Raw en-face OCT images.** (1-4) OCT images from different Z coordinate values separated by 40 μm along Z direction. (5) Superposition of 10 images separated by 10 μm along Z-direction, where the height position along Z is color-coded. Black color means no signal.

transferred to a PC for signal processing.

Fig. 4 shows *en-face* OCT images from 4 positions z separated by 40 μm . The coin was slightly tilted, and therefore the narrow axial resolution led to fragmented *en-face* OCT images. The 5th image underneath represents a summation of 10 *en-face* images separated 10 μm into a single projection, where the height in Z of each image was color-coded. The thickness of the bright patch in the *en-face* OCT images represents a projection of the axial resolution interval along the tilted surface of the coin. To widen the bright patch, the tilt of the coin in the volume of data acquired has been compensated by software means and two such tilted cuts, corresponding to the Z-position of the coin base (a) and the top of the letters (c) are shown in Fig. 5. Fig. 5(b1–b3) shows three B-scan OCT images. These are perpendicular to the *en-face* OCT images in Fig. 5(a) and oriented along the dashed lines superposed on the same image. The images in Fig. 4–5 confirm that the axial range is sufficient to cover the tilt of the coin and the height of the letters on the coin. Topography of the 3D volume generated is shown in Fig. 6. Due to the sinusoidal shape of the signal driving the KTN deflector, the images present a nonlinear variation of pixel size along the x -line in the raster. Therefore, margins were cropped to eliminate the regions of flyback. Considering the numerical values for the axial range and axial resolution evaluated above, a number of points $N_z = \Delta z / \delta z = 53$ along the depth coordinate is obtained. Therefore, using one half of KTN ramp, the acquired volume contains 200 x 250 x 53 voxels.

IV. CONCLUSION

This work responds to the progress in the high sweeping speed of modern tuning lasers. Galvanometer and resonant scanners are widely used in OCT instruments, however, when paired with a fast sweeping optical source, the distance between successive lateral pixels becomes smaller than the

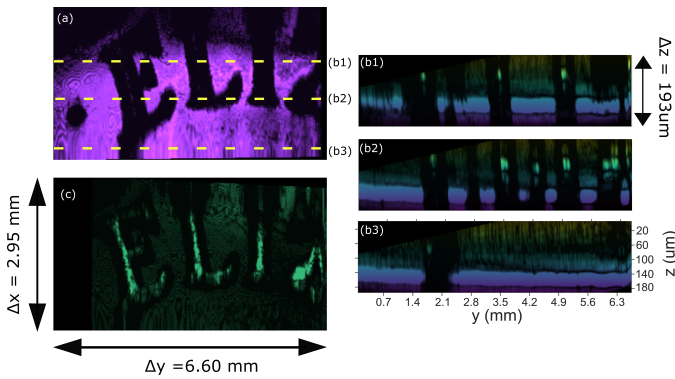


Fig. 5. **Tilt corrected OCT images.** (a) *En-face* image of the bottom of the letters. (b1-3) B-scans at lateral positions as indicated by dashed yellow lines in (a). (c) *En-face* image of the top of the letters.

optical transversal resolution, which effectively turns into data oversampling with no effective increase in the volume acquisition rate. The effective scanning procedure using a fast KTN-based scanner shown in this report demonstrated a volume production rate of up to 400 Hz, which is multiple times faster than reported with OCT scanning systems operating in the 1 μm band. The high-volume rate obtained here will provide less distortion due to movement when used with moving targets, it could also benefit several applications such as: phase-sensitive OCT, 4D-OCT, etc... [13]. However, increasing the sweeping speeds comes at the expense of limited sensitivity. With a duty cycle $\sim 50\%$, operating at 40 MHz repetition rate, this corresponds to an equivalent sweeping at 80 MHz with 100 % duty cycle. According to the estimated formula for sensitivity with the sweeping speed in De Boer, et al. [14], a 30 dB reduction in sensitivity was estimated due to the increase in the sweeping rate from 1 MHz to 100 MHz. This comparison does not yet consider larger noise levels owing to increase in the electronic bandwidth by 80 times when the sweeping rate is increased from 1 to 80 MHz. For instance, in a previous report Klein et al. [13], obtained a sensitivity of 90 dB at a sweeping rate of 1 MHz. Therefore, by taking into account two corrections: (i) suggested in [14] and (ii) due to enlarged noise bandwidth may lead to sensitivity values close to the >45 dB sensitivity reported here. If a fast system as described would be used on biological tissue, different avenues should be explored to enhance its sensitivity, for example, by using a much larger optical power or coherent averaging [15]. Care was taken in assembling a low noise swept source, compared with classical supercontinuum sources based on solitons, the coherent supercontinuum mechanism used in this report led to a reduced excess photon noise given by the relative intensity noise. Despite this, it was also found that the balanced detection scheme was unable to fully remove deterministic noise in the range of 3 – 5 GHz which will require further investigations. Another limitation of the instrument reported is given by the data acquisition. Although digital sampling acquisition is able to cope with tens of GHz, such high electrical bandwidths when combined with a dynamic range of 12 bits leads to a large volume of data. Due to the limited transfer speed and data processing time required, this prevents real-time

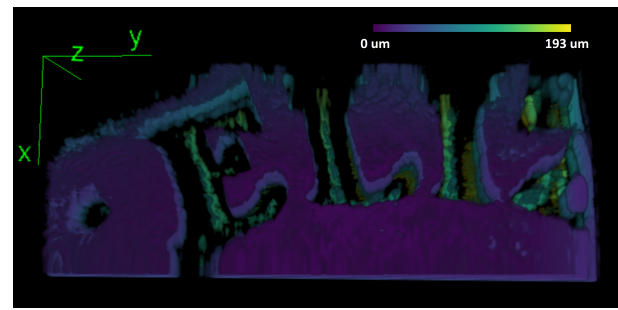


Fig. 6. **Topographical representation of a 3D volume** generated in a raster at 400 Hz from the coin, where the colorbar is used to illustrate the Z coordinate.

delivery of images. Improvements in reducing deterministic noise of fast sweeping sources accompanied by a better trade-off between sweeping time and volume acquisition time could enable system architecture as described here, to benefit both biomedical and industrial applications.

REFERENCES

- [1] D. Huang, F. Li, Z. He, Z. Cheng, C. Shang, and P. K. A. Wai, "400 MHz ultrafast optical coherence tomography," *Optics Letters*, vol. 45, no. 24, pp. 6675–6678, Dec. 2020.
- [2] J. P. Kolb, T. Klein, W. Wieser, W. Draxinger, and R. Huber, "Full volumetric video rate OCT of the posterior eye with up to 195.2 volumes/s," in *Optical Coherence Tomography and Coherence Domain Optical Methods in Biomedicine XIX*, vol. 9312. SPIE, 2015, pp. 11–17.
- [3] E. Auksoorius, D. Borycki, P. Stremplewski, K. Liżewski, S. Tomczewski, P. Niedźwiedziuk, B. L. Sikorski, and M. Wojtkowski, "In vivo imaging of the human cornea with high-speed and high-resolution Fourier-domain full-field optical coherence tomography," *Biomedical Optics Express*, vol. 11, no. 5, pp. 2849–2865, 2020.
- [4] M. Ohmi, Y. Shinya, J. Miyazu, S. Toyoda, and T. Sakamoto, "High-Speed Time-Domain En Face Optical Coherence Tomography System Using KTN Optical Beam Deflector," *Optics and Photonics Journal*, vol. 9, no. 5, pp. 53–59, May. 2019.
- [5] Y. Sasaki, Y. Okabe, M. Ueno, T. Sakamoto, S. Toyoda, J. Kobayashi, S. Yagi, and K. Naganuma, "High-speed KTN optical beam deflector for swept-source optical coherence tomography," in *2013 3rd IEEE CPMT Symposium Japan*. IEEE, 2013, pp. 1–4.
- [6] S. Moon and D. Y. Kim, "Ultra-high-speed optical coherence tomography with a stretched pulse supercontinuum source," *Optics Express*, vol. 14, no. 24, pp. 11 575–11 584, Nov. 2006.
- [7] X. Wei, A. K. S. Lau, Y. Xu, K. K. Tsia, and K. K. Y. Wong, "28 MHz swept source at 1.0 μm for ultrafast quantitative phase imaging," *Biomedical Optics Express*, vol. 6, no. 10, pp. 3855–3864, Nov. 2015.
- [8] S. Grelet, P. Bowen, P. M. Moselund, and A. Podoleanu, "80 MHz swept source operating at 1060 nm Based on All-Normal-Dispersion Supercontinuum Generation for Ultrahigh-speed Optical Coherence Tomography," in *European Conference on Biomedical Optics*. Optical Society of America, Jun. 2021, p. ETu3D5.
- [9] E. Genier, S. Grelet, R. D. Engelscholm, P. Bowen, P. M. Moselund, O. Bang, J. M. Dudley, and T. Sylvestre, "Ultra-flat, low-noise, and linearly polarized fiber supercontinuum source covering 670–1390 nm," *Optics Letters*, vol. 47, no. 8, pp. 1820–1823, Mar. 2022.
- [10] T. Imai, M. Ueno, Y. Sasaki, and T. Sakamoto, "Analyses of optical rays in KTN optical beam deflectors for device design," *Applied Optics*, vol. 56, no. 25, pp. 7277–7285, 2017.
- [11] S. Rivet, M. Maria, A. Bradu, T. Feuchter, L. Leick, and A. Podoleanu, "Complex master slave interferometry," *Optics Express*, vol. 24, no. 3, pp. 2885–2904, Feb. 2016.
- [12] A. Bradu, N. M. Israelsen, M. Maria, M. J. Marques, S. Rivet, T. Feuchter, O. Bang, and A. Podoleanu, "Recovering distance information in spectral domain interferometry," *Scientific Reports*, vol. 8, no. 1, pp. 1–16, Oct. 2018.
- [13] T. Klein, W. Wieser, L. Reznicek, A. Neubauer, A. Kampik, and R. Huber, "Multi-MHz retinal OCT," *Biomedical Optics Express*, vol. 4, no. 10, pp. 1890–1908, Aug. 2013.

- [14] J. F. D. Boer, B. Cense, B. H. Park, M. C. Pierce, G. J. Tearney, and B. E. Bouma, "Improved signal-to-noise ratio in spectral-domain compared with time-domain optical coherence tomography," *Optics Letters*, vol. 28, no. 21, pp. 2067–2069, Nov. 2003.
- [15] B. Baumann, C. W. Merkle, R. A. Leitgeb, M. Augustin, A. Wartak, M. Pircher, and C. K. Hitzenberger, "Signal averaging improves signal-to-noise in OCT images: But which approach works best, and when?" *Biomedical Optics Express*, vol. 10, no. 11, pp. 5755–5775, Nov. 2019.